A Numerical Analysis on the Curved Bileaflet Mechanical Heart Valve (MHV): Leaflet Motion and Blood Flow in an Elastic Blood Vessel

Jin Seok Bang
Mechanical Engineering Department, Graduate School of Kyunghee University, 1 Seochon, Kihung, Yongin, Kyunggi, 449-701, Korea
Choeng Ryul Choi
College of Environmental Engineering, An Yang University, Anyang 5-dong, Manan-gu, Anyang-shi, Kyunggi, 430-714, Korea
Chang Nyung Kim*
College of Advanced Technology, Kyunghee University, 1 Seochon, Kihung, Yongin, Kyunggi, 449-701, Korea

In blood flow passing through the mechanical heart valve (MHV) and elastic blood vessel, hemolysis and platelet activation causing thrombus formation can be seen owing to the shear stress in the blood. Also, fracture and deformation of leaflets can be observed depending on the shape and material properties of the leaflets which is opened and closed in a cycle. Hence, comprehensive study is needed on the hemodynamics which is associated with the motion of leaflet and elastic blood vessel in terms of fluid-structure interaction. In this paper, a numerical analysis has been performed for a three-dimensional pulsatile blood flow associated with the elastic blood vessel and curved bileaflet for multiple cycles in light of fluid-structure interaction. From this analysis fluttering phenomenon and rebound of the leaflet have been observed and recirculation and regurgitation have been found in the flow fields of the blood. Also, the pressure distribution and the radial displacement of the elastic blood vessel have been obtained. The motion of the leaflet and flow fields of the blood have shown similar tendency compared with the previous experiments carried out in other studies. The present study can contribute to the design methodology for the curved bileaflet mechanical heart valve. Furthermore, the proposed fluid-structure interaction method will be effectively used in various fields where the interaction between fluid flow and structure are involved.

Key Words: Mechanical Heart Valve (MHV), Artery, Thrombus Formation, Hemodynamics, Fluid-Structure Interaction (FSI)

Nomenclature

J : Coordinate transformation Jacobian
$\{q\}$: Displacement vector
$[M]$: Mass matrix
$[C]$: Damping matrix
$[K]$: Stiffness matrix
$\{F\}$: Force vector
$[IC]$: Influence coefficient
$\{p\}_b$: Pressure at fluid-structure boundaries

Greek Letters

ρ : Density
μ : Dynamic viscosity
θ : Leaflet opening angle
ϕ : Rotation angle

* Corresponding Author,
E-mail : cnkim@khu.ac.kr
TEL : +82-31-201-2578; **FAX** : +82-31-202-9715
College of Advanced Technology, Kyunghee University, 1 Seochon, Kihung, Yongin, Kyunggi 449-701, Korea.
(Manuscript **Received** December 10, 2004; **Revised** August 4, 2005)

1. Introduction

The human heart has four valves ; the aortic, mitral, tricuspid and pulmonary valves. The heart valves open to allow blood to be pumped forward, and they close to prevent blood from flowing backward. Human heart valves are formed by flaps of tissue called leaflets or cusps. Heart valve diseases are classified as congenital when some factor during fetal development causes the valve to form abnormally, and acquired if malfunction occurs in a valve that was structurally normal at birth. For congenital heart valve disease, many researchers suppose that many cases are caused by inherited factors. Some common causes of acquired heart valve diseases include that rheumatic fever (an inflammatory illness that may follow an untreated streptococcus throat infection), endocarditis (inflammation and infection of the heart valves) and idiopathic calcific aortic stenosis (degenerative condition seen in the elderly, in which the aortic valve cusps become thickened, fused and infiltrated with calcium). As calcium deposits accumulated, they can restrict the motion of the leaflets. Therefore, either stenosis where the leaflets can no longer open suitably, or regurgitation where the leaflets can no longer close properly and some blood leaks back into the atrium with each beat is caused.

In these cases, surgical procedure called valvotomy, valvuloplasty, or valve repair is performed. Nevertheless a valve is so seriously deformed or diseased, it has to be replaced with an artificial heart valve (Choi et al., 2001 ; 2003). When a patient requires a heart valve replacement, there are two types of available artificial valves. One is a mechanical heart valve (MHV) and the other is a bioprosthetic heart valve (BHV). A mechanical heart valve which is most commonly used MHV in the aorta is shown in Fig. 1.

Here, mechanical heart valves have merits of nice performance and reliable durability. Mechanical heart valves usually last throughout the lifetime of patient and do not required valve replacement. On the other hand, as mechanical heart valves are made of metal or plastic, patients

(a) (b)

Fig. 1 The MHV model (a) components of bileaflet mechanical heart valve (Edward TEKNA™) (b) side view of installed MHV in the aorta

are required to take anticoagulation medication throughout their lifetime to prevent the thrombus formation. One aspect of particular concern with the normal function of mechanical heart valve is that they can generate turbulence in the blood flow, since it has been related to thrombus formation (Stein et al., 1974 ; Edmunds, 1982 ; Mauro et al., 2001). The second problem entailed by the mechanical heart valve yielding alteration of the cardiovascular environment's fluid dynamics is hemolysis, which has been studied extensively with regard to the critical value of Reynolds shear stress which may cause red blood cell damage or platelet activation (Paul et al., 1999 ; Mauro et al., 2001).

Many important aspects of hemodynamic aortic blood flow have been investigated in experimental studies (Skalak, 1982 ; Farahifar et al., 1985 ; Chandran et al., 1985 ; Rosseau et al., 1984 ; Sallam et al., 1976 ; Tillman et al., 1984 ; Yoganathan et al., 1979 ; Woo et al., 1986), but sometimes these studies lack spatial resolution, have problems analyzing transient phenomena or partially lack the detailed observation of theoretical modeling because the pressure and the velocities of the blood are hard to measure (Krafczyk et al., 1998). Numerical analysis has indeed led to a better understanding of the characteristics of blood flow and has allowed medical hemodynamicists to gain an improved understanding of the motion of containing structures (vessel and leaflet) as well as the contained blood flow (Krafczyk et al., 1998).

In this study, investigation on the flow fields of the blood flowing through the curved bileaflet mechanical heart valve has been performed with fluid-structure interaction method, and the shortcomings of previous MHV studies where the leaflet motion has been ignored or simplified, have been overcome. A numerical analysis with the fluid-structure interaction between the blood flow and the motion of leaflets in an elastic blood vessel has been carried out in order to calculate the blood flow through the curved bileaflet mechanical heart valve.

2. Mathematical Modeling

2.1 Governing equations for blood flow

The governing equations for a blood flow of a Newtonian-fluid (Krafczyk et al., 1998 ; De Hart et al., 2000) are the continuity equation and the Navier-Stokes equation for an incompressible fluid, which can be written in a strong conservation form in curvilinear coordinates as follows :

$$\frac{\partial}{\partial t}\left(\frac{\rho}{J}\right)+\frac{\partial}{\partial \zeta^j}\left(\frac{\rho U_j}{J}\right)=0 \tag{1}$$

$$\begin{aligned}&\frac{\partial}{\partial t}\left(\frac{\rho u_i}{J}\right)+\frac{\partial}{\partial \xi^j}\left(\frac{\rho U_j u_i}{J}\right)\\&=-\frac{1}{J}\frac{\partial \xi^j}{\partial x_i}\frac{\partial p}{\partial \xi^j}+\frac{\partial}{\partial \xi^k}\left[\frac{\mu}{J}\frac{\partial \xi^k}{\partial x_j}\left(\frac{\partial \xi^l}{\partial x_j}\frac{\partial u_i}{\partial \xi^l}+\frac{\partial \xi^l}{\partial x_i}\frac{\partial u_j}{\partial \xi^l}\right.\right.\\&\qquad\left.\left.-\frac{2}{3}\delta_{ij}\frac{\partial u_l}{\partial \xi^m}\frac{\partial \xi^m}{\partial x_l}\right)\right]\end{aligned} \tag{2}$$

where, u_i is the Cartesian velocity component, x_i the Cartesian coordinate, U_j the velocity component in the ξ^j direction (contra-variant velocity component), and J the coordinate transformation Jacobian. Further,

$$x_1=x,\ x_2=y,\ x_3=z,\ \xi^1=\xi,\ \xi^2=\eta,\ \xi^3=\zeta \tag{3}$$

$$U_j=\frac{\partial \xi^j}{\partial t}+\frac{\partial \xi^j}{\partial x_i}u_i=0 \tag{4}$$

where, $\frac{\partial \xi^j}{\partial t}$ represents the grid velocity, so that the above formulation is in an Eulerian-Lagrangian frame.

2.2 Governing equations for structural dynamics

The finite element formulation of the structural dynamics equation can be generally written in a linear form follows :

$$[M]\{\ddot{q}\}+[C]\{\dot{q}\}+[K]\{q\}=\{F\} \tag{5}$$

where, $\{q\}$, $[M]$, $[C]$, $[K]$ and $\{F\}$ are the displacement vector, the mass matrix, the damping matrix, the stiffness matrix, and the force vector caused by the fluid dynamic load and shear stresses, respectively.

$$[M]=\sum m_{ij}^e=\sum\int N_i\rho_s N_j dv \tag{6}$$

$$[C]=\sum C_{ij}^e=\sum\int N_i\mu_s N_j dv \tag{7}$$

$$[K]=\sum k_{ij}^e=\sum\int B_i D_{ji} B_j dv \tag{8}$$

$$\{F\}=\sum\{f_i\}^e=\sum\int N_i p dv \tag{9}$$

where, N_i, ρ_s, μ_s and D_{ij} are the shape function, the density of the structure, the damping parameter and the elasticity matrix. B_i is related to N_i through a linear operator L_{ij} :

$$B_i=L_{ij}N_j \tag{10}$$

Newmark's scheme is applied to solve the above Eq. (5). For the known values of q, $\dot{q}$, $\ddot{q}$ at (n-1) th time step, we have

$$\{q\}=\frac{2}{\Delta t}\left[[K]+\frac{4}{\Delta t^2}[M]+\frac{4}{\Delta t}[C]\right]^{-1}\{F\}+\{E\} \tag{11}$$

where, $\{E\}$ comprises all the terms of q^{n-1}, $\dot{q}^{n-1}$ and $\ddot{q}^{n-1}$.

2.3 Coupling of fluid and structure

In Eq. (2) of fluid dynamics, the structural effect comes into play only through the grid velocity term. This section will discuss the implicit coupling procedure. It is known that at the fluid-structure interface, fluid velocity is always equal to the structure velocity and the contra-variant velocity component in the Eulerian-Lagrangian formulation is zero :

$$U_j=\frac{\partial \xi^j}{\partial t}+\frac{\partial \xi^j}{\partial x_i}u_i=0 \tag{12}$$

If $\{\dot{q}\}_b$ is the velocity of structure at the fluid-structure interface, then

$$\{\dot{q}\}_b=\frac{\partial\xi^j}{\partial t}=\frac{\partial\xi^j}{\partial x_i}u \tag{13}$$

On the other hand, Eq. (8) can be expressed in the following perturbation form :

$$\{\dot{q}\}'_b=[IC]\{p\}'_b \tag{14}$$

In view of Eq. (9), we have

$$\frac{\partial\xi^j}{\partial x_i}u'_i=[IC]\{p\}'_b \tag{15}$$

where, $[IC]$ and $\{p\}_b$ are the influence coefficient (Yang et al., 1994; Choi, 2003) and the pressure at the fluid-structure interface, respectively. When Eq. (15) is substituted into the pressure gradient term of the pressure correction equation, the resulting equation depends only on flow variables.

3. Numerical Analysis

Using the fluid-structure interaction method, the blood flow, the motion of the leaflet and the elastic blood vessel have been analyzed concurrently. In modeling fluid-structure interaction, the fluid domain is most conveniently described with respect to an Eulerian reference frame (material moves through the computational domain) while a Lagrangian formulation (computational domain moves with the material) is more appropriate for the structure domain (De Hart et al., 2000). To consider both fluid and structure domain concurrently, in this study, Eulerian-Lagrangian formulation has been used. A finite volume computational fluid dynamics code and a finite element structure dynamics code have been used for the flow and structure equation respectively. To solve these equations, upwind differencing SIMPLEC scheme has been used in the flow solver and a commercial software package CFD-ACE+ version 6.4 and FEMSTRESS which is a finite element structural analysis module have been adopted.

The model of the mechanical heart valve (Edward TEKNA™) used for the current calculation is shown in Figs. 2 and 3.

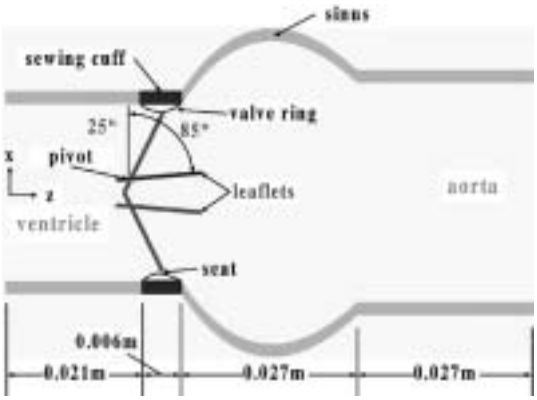

Fig. 2 The geometry drawn in x-z plane used in the current analysis

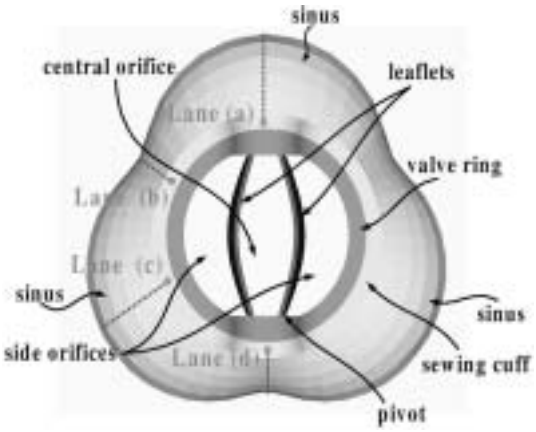

(a)

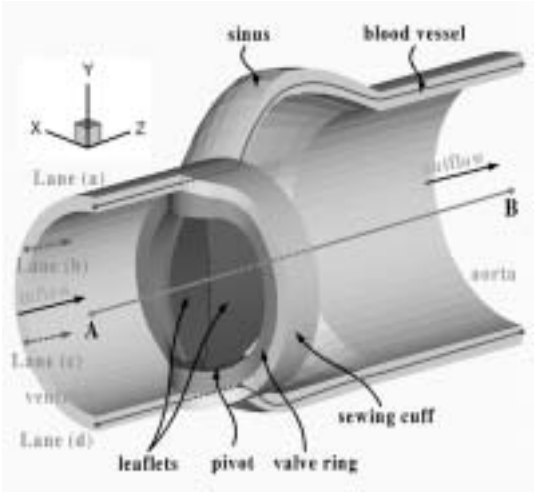

(b)

Fig. 3 Configuration of the calculation model (a) front view (b) bird-eyes view

The blood has been assumed to be a Newtonian fluid, and the density ρ is 1,000 kg/m^3, and the dynamic viscosity μ is 3.5×10^{-3} kg/m·s. The diameters of a ventricular and an aortic blood vessel have been assumed to be 25 mm and 33.48 mm, respectively. For mechanical heart valve the thickness of the leaflet is 0.65 mm and the inside diameter is 22.3 mm. Opening angles of the leaflet have been set to be $25°<\theta<85°$ (Fig. 2). The geometry of the downstream region of mechanical heart valve includes the Sinus of Valsalva model. The pressure waveforms, measured in vitro (Thubrikar et al., 1996a; 1996b) in the ventricle and the aorta with 75 beats per minute, have been used as pressure boundary conditions for the numerical calculation (Fig. 4).

At the vessel surface, no slip condition has been employed for the blood flow and the velocity of the blood at the leaflet surface is identical to that of the leaflet surface. Sewing cuff region which is not related with the blood flow has been regarded as the blood vessel which only connects the ventricle and the end region of aorta and this region is fixed without any displacement in the calculation.

In the numerical calculation of the current formulation, a grid system of 28512 grids have been chosen after many times of test running for different grid systems with different grid number, when the choice of the time step size is to be under consideration together. The time step size of $\Delta t=0.0005$ s has been used when the structure (the leaflet) is moving while the time step size of $\Delta t=0.01$ s has been employed when the structure is not moving. However, when the leaflet is rebounding from the seat and the blood velocity is very high (at the end of the closing phase of the leaflet) the time step size of $\Delta t=0.00005$ s has been adopted. Of course, a smooth change of the time step size has been used in the transition between different phases.

4. Results and Discussion

4.1 Motion of a curved bileaflet mechanical heart valve

Transient variation of the leaflet opening angle with the interaction model between the blood flow and the leaflet motion is obtained and plotted in Fig. 5.

The motion of the leaflet can be divided into four phases; fully closed phase (10~1), opening phase (1~5), fully opened phase (5~6), closing phase (6~10). In the opening phase, according to the systole, pressure of the ventricle is increased and the blood flows into the aorta. Here, the leaflet is opened slowly at the beginning, but as the time goes on opening velocity of the leaflet becomes faster increasingly than it is at the beginning and then at the end stage of opening phase the leaflet arrives at the maximum opening angle (time position (5) at $t=0.209$ s, $\theta=85°$).

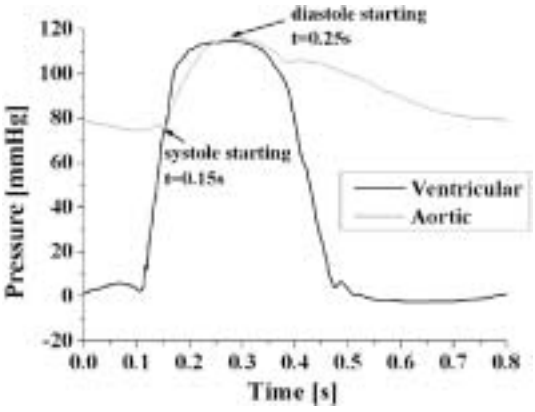

Fig. 4 Transient pressure waveforms adopted as boundary conditions

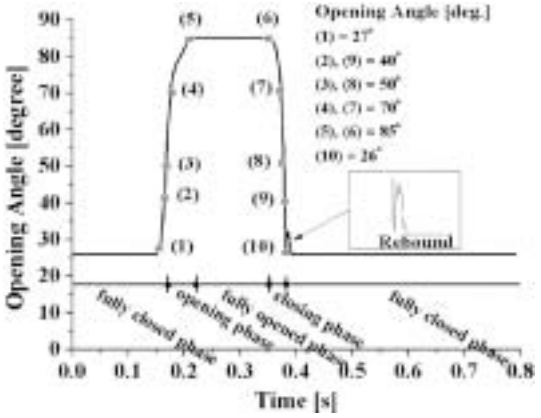

Fig. 5 Transient variation in the opening angle of the leaflet

Though fluttering phenomenon is detected infinitesimally, the leaflet maintains generally maximum opening angle in the fully opened phase. The ventricular diastole starts at $t=0.25$ s, but actually the closing phase starts at $t=0.35$ s. Hence, it can be noted that there is a time delay. When considering the period of time for the opening and closing phase, it takes 0.055 s for the opening phase and 0.03 s for the closing phase. When the leaflet starts to contact with the valve ring, rebound of the leaflet takes place because of the inertia effect of the motion of the leaflet and water hammer effect. The general characteristics of the motion of the leaflet are similar to the result obtained by CFD analysis using fluid-structure interaction method for the case of inelastic vessel wall by Choi et al.(2003).

4.2 Flow fields for a curved bileaflet mechanical heart valve

Velocity vector profiles in the different time positions at the mid plane are shown in Fig. 6.

In the opening phase, the blood flows mainly through side orifices between the leaflet and valve ring. In the fully opened state (time position (5) at $t=0.209$ s, $\theta=85°$), in the valve (Fig. 6(c))

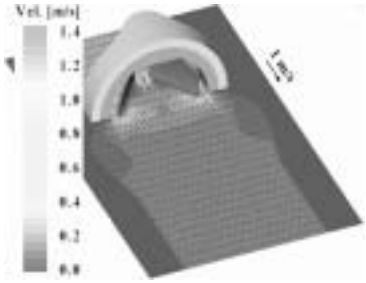

Time position (3) at $t=0.167$s, $\theta=50°$
(a)

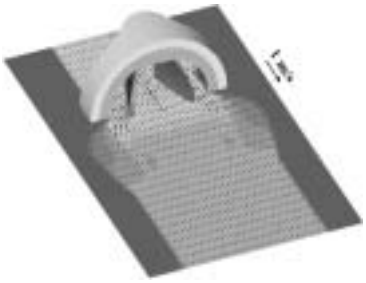

Time position (4) at $t=0.175$s, $\theta=70°$
(b)

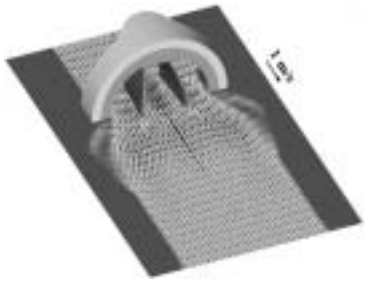

Time position (5) at $t=0.209$s, $\theta=85°$
(c)

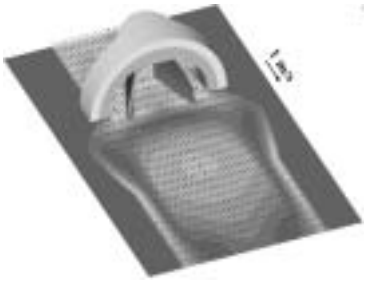

Time position (7) at $t=0.373$s, $\theta=70°$
(d)

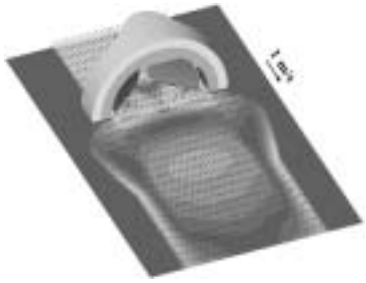

Time position (9) at $t=0.379$s, $\theta=40°$
(e)

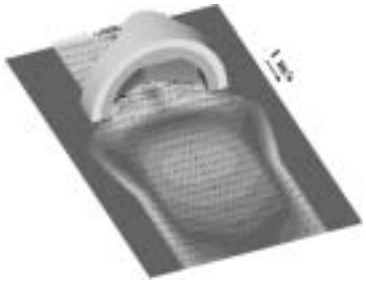

Time position (10) at $t=0.380$s, $\theta=26°$
(f)

Fig. 6 Transient velocity vectors of the blood flow in the mid plane

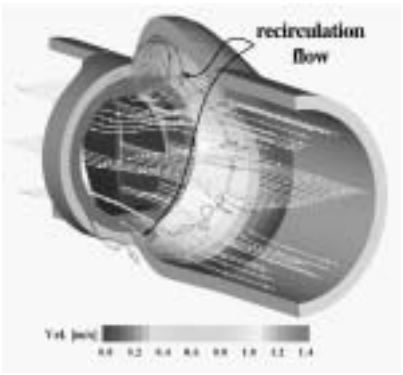

Fig. 7 Streamlines in the fully opened phase (time position (5) at $t=0.209$ s, $\theta=85°$)

observed are three flows of high velocities; two flows through the side orifices, one flow through the central orifice. Also, some streamlines are shown in Fig. 7 at this moment.

In this figure, recirculation flows are shown in the sinus region and higher velocities are found in between the two leaflets (i.e., in the central orifice). The closing motion of the leaflet is generated by reverse pressure gradient which is caused by diastole. During the closing phase (Fig. 6(d)~(f)), the reverse flow is formed in the region close to the leaflet, ring, and sinus wall. As a whole, flow fields shown in this paper are

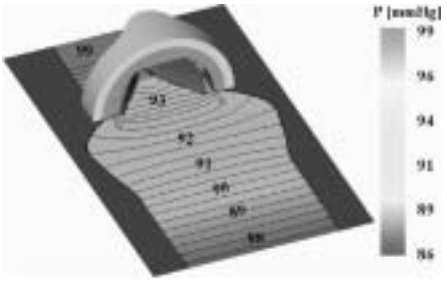

Time position (3) at $t=0.167$s, $\theta=50°$
(a)

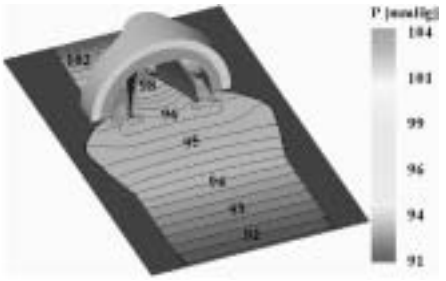

Time position (4) at $t=0.175$s, $\theta=70°$
(b)

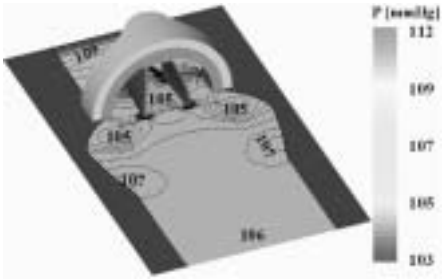

Time position (5) at $t=0.209$s, $\theta=85°$
(c)

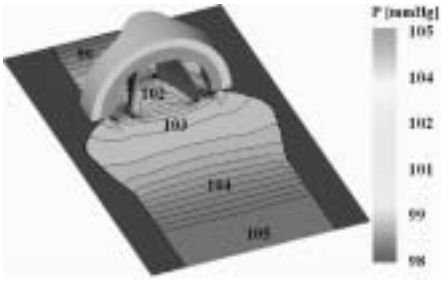

Time position (7) at $t=0.373$s, $\theta=70°$
(d)

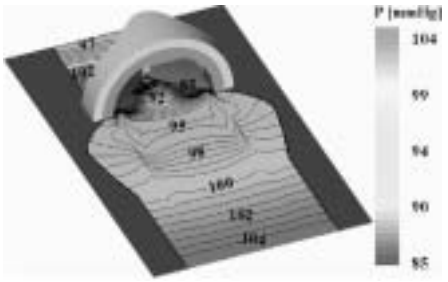

Time position (9) at $t=0.379$s, $\theta=40°$
(e)

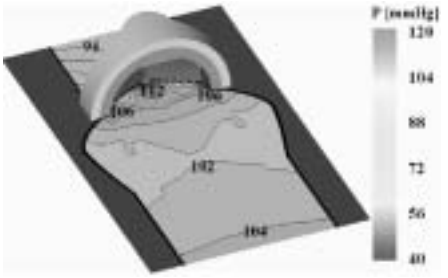

Time position (10) at $t=0.380$s, $\theta=26°$
(f)

Fig. 8 Transient pressure distribution profiles in the mid plane

similar to that of the experimental study performed by Woo et al.(1986) for a pulsatile flow.

4.3 Pressure fields for a curved bileaflet mechanical heart valve

Pressure distributions in the different time positions in the mid plane are shown in Fig. 8.

During the opening phase of the leaflet shown in Fig. 8(a)~(c), the pressure of ventricular region is higher and that of aortic region is lower. Though the pressure gradient is relatively small in the beginning of the opening phase, pressure drop is increased in the flow direction when the opening angle grows larger. When the leaflets are fully opened (time position (5) at $t=0.209$ s, $\theta=85°$), because of higher velocities observed in the three jets together with the geometrical characteristics of the sinus, lower pressures are found in the central orifice and in the upstream region of the sinus. The variation of pressure profiles along the center line (along the line A-B in Fig. 3(b)) is shown in Fig. 9 for different opening angles of the leaflet.

When the leaflets are fully closed (time position (10), $t=0.380$s, $\theta=26°$), velocity vectors and pressure distribution are shown in Fig. 10. In this state, higher pressure is formed in the vicinity of aortic side of the leaflet while lower pressure is formed in the vicinity of ventricular side of the leaflet. For one cycle ($t=0.8$ s), when the leaflet is almost closed, the largest pressure gradient is detected in the ventricle region and the lowest pressure is observed near the seat in association with the fact that the blood regurgitates rapidly from the aorta region toward the ventricle through the narrow gap between the edge of leaflet and the seat. It can be expected that red blood cells may be damaged by large shear stress caused by high velocity in the narrow gap at this time, with higher possibility of the cavitation at lower pressure (Giersiepen et al., 1984).

4.4 The characteristics of the motion of an elastic blood vessel

In this study, the radial displacements of the elastic blood vessel are calculated along the four lanes of the vessel. As the aortic and the ventricular boundary surface located at both the ends of the elastic blood vessel are fixed and the sewing cuff region is of solid domain, the radial displacements are zero at both the ends and in the sewing cuff region.

The radial displacements of the elastic blood vessel at different time positions are obtained and plotted in Fig. 11 and the maximum radial displacements (MRDs) at the time positions along the lanes (a)~(d) denoted in Fig. 3 are listed in Table 1.

Both the lanes (a) and (d) are laid along the z-direction (chord length) of the elastic blood vessel (in Fig. 3), but because of the sinus on the lane (a), the MRD of the two lanes are detected

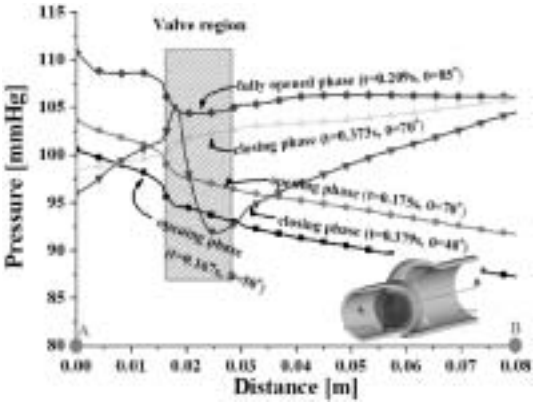

Fig. 9 Pressure profiles along the axial distance at different time positions

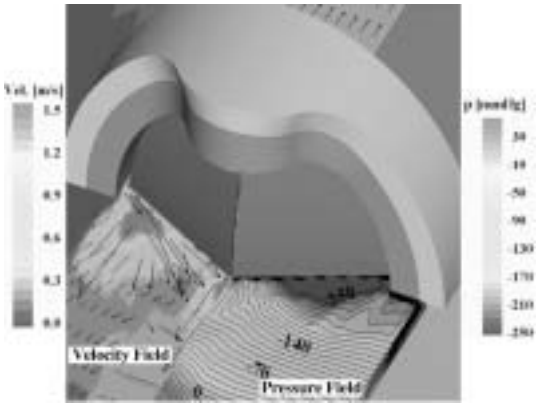

Fig. 10 Velocity vectors and pressure distribution (time position (10) at $t=0.380$ s, $\theta=26°$)

differently. The MRDs of lanes (b) and (c), the position of which are rotated by $\phi=60°$ and $\phi=120°$ from the lane (a), respectively, are similar to those of the lane (d) and (a), respectively.

Though on the ventricular blood vessel region (upstream region), the radial displacements of the lanes (b) and (c) are approximately larger about two times than those of the lanes (a) and (d), but in the aortic blood vessel region the radial displacement of the lanes (b) and (d) are larger about three times than those of the lanes (a) and (c). The radial displacements of the upstream region are expected to be characterized by the direction of the pivots of the leaflets. Therefore, the displacement characteristics along the lanes (b) and (c) are very similar and those along the lanes (a) and (b) are almost the same, respectively. However, the radial displacement of the downstream are expected to be characterized by the existence of the sinus. Therefore, the radial displacement of the lanes (b) and (d), which do not pass through the sinus, are larger than those of the lanes (a) and (c).

While the opening angle of the leaflet grows up, the radial displacements of each lane are increased as shown at the time positions (1) ~ (5)

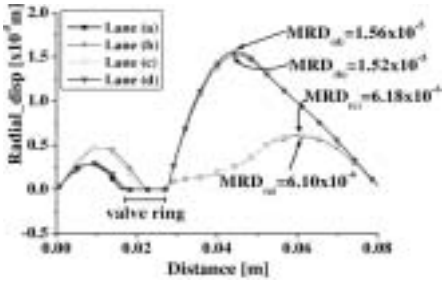

Time position (3) at $t=0.167$s, $\theta=50°$

(a)

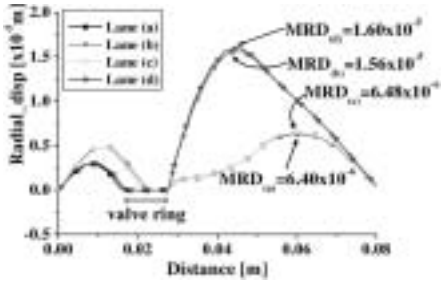

Time position (4) at $t=0.175$s, $\theta=70°$

(b)

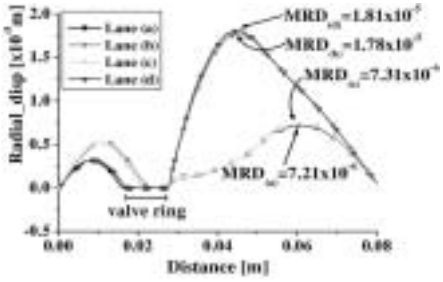

Time position (5) at $t=0.209$s, $\theta=85°$

(c)

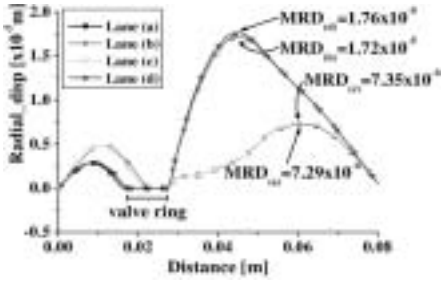

Time position (7) at $t=0.373$s, $\theta=70°$

(d)

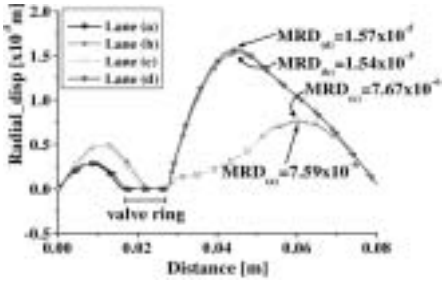

Time position (9) at $t=0.379$s, $\theta=40°$

(e)

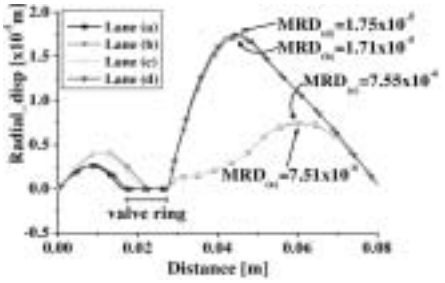

Time position (10) at $t=0.380$s, $\theta=26°$

(f)

Fig. 11 Radial displacements of the blood vessel along the lanes (a) ~ (d)

Table 1 Maximum radial displacements (MRDs) at different time positions

Time Position	Maximum Radial Displacements (MRDs) [$\times 10^{-5}$ m]			
	Lane (a)	Lane (b)	Lane (c)	Lane (d)
(1)	0.534	1.279	0.540	1.308
(2)	0.594	1.476	0.601	1.511
(3)	0.610	1.523	0.618	1.558
(4)	0.640	1.561	0.648	1.597
(5)	0.721	1.775	0.731	1.811
(6)	0.771	1.784	0.777	1.828
(7)	0.729	1.720	0.735	1.763
(8)	0.706	1.733	0.711	1.776
(9)	0.759	1.535	0.767	1.570
(10)	0.751	1.713	0.755	1.751

in Fig. 11. Before the leaflet gets into closing phase, the maximum radial displacement of the elastic blood vessel is observed (at the time position (6), $t=0.350$ s, $MRD_{(d)}=1.828\times10^{-5}$ m) and the MRDs of the lanes (b), (d) and the lanes (a), (c) are observed at the position of 17.32 mm and 31.42 mm downstream from the valve ring, respectively. In the closing phase (time positions (7) ~ (9)), the $MRD_{(b)}$ and $MRD_{(d)}$ are decreased. But when the leaflet is fully closed (time position (10)), the $MRD_{(b)}$ and $MRD_{(d)}$ are increased again in association with the increase of the local blood pressure with the closure of the leaflets. Although the displacement of the lanes (a) and (c) are increased slightly at the time position (9), they are decreased at the time position (10).

The configuration and position of valve have an effect on the features of the radial displacements. And the structural characteristics of mechanical heart valve is different from those of tissue valve, it can be expected that the radial displacements of the blood vessel with mechanical heart valve are different from that with tissue valve. The MRDs are caused in association with the pressure distribution mainly.

5. Conclusions

In this paper, a numerical analysis has been performed for the blood flow which interacts with the motion of the leaflet and the blood vessel in the curved bileaflet mechanical heart valve with fluid-structure interaction method. Here, the detailed features of the blood flow and the leaflet motion have been obtained together with the characteristics of the radial motion of the blood vessel. This study has overcome the shortcomings of previous MHV studies where it has been assumed that the blood vessel was non-elastic and the motion of the leaflet has been ignored or simplified. In the current study adopting fluid-structure interaction method, in other to solve the flow and the structure equations simultaneously, a finite volume computational fluid dynamics code and a finite element structure dynamics code have been used concurrently.

When the leaflet is fully opened, fluttering phenomenon has been detected in association with the blood flow. And when the leaflet starts to contact with the valve ring, the rebound of the leaflet takes place. Also when the leaflet is fully opened, recirculation flows have been observed in the sinus region. During the closing phase, regurgitation has been formed between the ring and the edge of the each leaflet. In consideration of the entire domain, the pressure drop occurs mainly in the valve region. While the opening angle of the leaflet grows up, the radial displacements of the vessel increases and just before the leaflet starts closing phase, the MRDs of the elastic blood vessel have been observed.

The present results have shown similar tendency to those obtained by previous experiments for flow fields, and can contribute to the design methodology for the curved bileaflet mechanical heart valve. Furthermore, the proposed fluid-structure interaction method will be effectively used in various fields where the interaction between fluid flow and structure is involved.

Acknowledgments

This study was financially supported by the KOREA SCIENCE AND ENGINEERING FOUNDATION (Project number : R05-2002-000-00990-0).

References

Chandran, K. B., Khalighi, B. and Chen, C. J., 1985, "Experimental Study of Physiological Pulsatile Flow Past Valve Prostheses in a Model of Human Aorta-II. Tiling Disc Valves and the Effect of Orientation," *Journal of Biomechanics*, Vol. 18, No. 10, pp. 773～780.

Choi, C. R. and Kim, C. N., 2001, "Characteristics of Transient Blood Flow in MHVs with Different Maximum Opening Angles Using Fluid-Structure Interaction Method," *Korean J. Chem. Eng.*, Vol. 18, No. 6, pp. 809～815.

Choi, C. R., 2003, "An Experimental and Numerical Analysis on Transient Three-dimensional Flow Fields through Bileaflet Mechanical Heart Valve (MHV) using Particle Image Velocity (PIV) and Fluid-Structure Interaction (FSI) Model," *Ph.D. dissertation*, Kyunghee University, Korea.

Choi, C. R., Kim, C. N., Kwon, Y. J. and Lee, J. W., 2003, "Pulsatile Blood Flows Through a Bileaflet Mechanical Heart Valve with Different Approach Methods of Numerical Analysis ; Pulsatile Flows with Fixed Leaflets and Interacted with Moving Leaflets," *KSME International Journal*, Vol. 17, No. 7, pp. 1073～1082.

De Hart, J., Peters, G. W. M., Schreurs, P. J. G. and Baaijens, F. P. T., 2000, "A Two-Dimensional Fluid-Structure Interaction Model of the Aortic Value," *Journal of Biomechanics*, Vol. 33, pp. 1079～1088.

Edmunds Jr., L. H., 1982, "Thromboembolic Complication of Current Cardiac Valvular Prostheses," *Annals in Thoracic Surgery*, Vol. 34, pp. 96～106.

Farahifar, D., Cassot, F. and Bodard, H., 1985, "Velocity Profiles in the Two Prosthetic Heart Valves Using a New Cardiovascular Simulator," *Journal of Biomechanics*, Vol. 18, No. 10, pp. 789～802.

Giersiepen, M., Wurzinger, L. J., Opitz, R. and Reul, H., 1984, "Estimation of Shear Stress Related Blood Damage in Heart Valve Prostheses in Vitro Comparison of 25 mm Aortic Valves," *Int. J. of Artificial Organs*, Vol. 13, No. 5, pp. 300～306.

Krafczyk, M., Cerrolaza, M., Schulz, M. and Rank, E., 1998, "Analysis of 3D Transient Blood Flow Passing Through an Artificial Aortic Valve by Lattice-Boltzmann Methods," *Journal of Biomechanics*, Vol. 31, pp. 453～462.

Mauro, G., Carla, D., Giuseppe, D. and Vincenzo, B., 2001, "The Influence of the Leaflets' Curvature in the Flow Fields in Two Bileaflet Prosthetic Heart Valves," *Journal of Biomechanics*, Vol. 34, pp. 613～621.

Paul, R., Schugner, F., Reul, H. and Rau, G., 1999, "Recent Findings in Flow Induced Blood Damage : Critical Shear Stresses and Exposure Times Obtained with a High Shear Couette-System," *Artificial Organs*, Vol. 23, No. 7, pp. 680～688.

Rosseau, E. P. M., Van de Ven, A. P. C., Van Steenhoven, A. A. and Seroo, J. M., 1984, "Design of a System for the Accelerated Loading of Heart Valve Prostheses," *Journal of Biomechanics*, Vol. 17, No. 2, pp. 145～153.

Sallam, I. A., Shaw, A. and Bain, W. H., 1976, "Experimental Evaluation of Mechanical Haemolysis with Starr-Edwards, Kay-Shiley and Bjork-Shiley valves," *Scandinavian Journal of Thoracic and Cardiovascular Surgery*, Vol. 10, pp. 117～122.

Skalak, R., 1982, "Finite Elements in Biofluid," *FE Analysis in Biomechanics*.

Stein, P. D. and Sabbah, H. N., 1974, "Measured Turbulence and Its Effect in Thrombus Formation," *Circulation Research.*, Vol. 35, pp. 608～614.

Thubrika, M. J., Selim, G., Robicsek, F. and Fowler, B., 1996a, "Effect of the Sinus Geometry on the Dynamics of Bioprosthetic Heart Valves (abstract)," *Ann. Biomed. Eng.*, Vol. 24, S3.

Thubrika, M. J., Selim, G., Robicsek, F. and Fowler, B., 1996b, "Effect of the Sinus Geometry on the Dynamics of Bioprosthetic Heart Valves (abstract)," *Proceedings of the 18th Annual International Conference of the IEEE Engineering in Medicine and Biology Society Amsterdam*, The Netherlands, pg. 10, November.

Tillman, W., Reul, H., Herold, M., Bruss, K. H. and Van Gilse, J., 1984, "In Vitro Wall Shear

Measurements at Aortic Valve Prostheses," *Journal of Biomechanics*, Vol. 17, No. 4, pp. 263~279.

Woo, Y. R. and Yoganathan, A. P., 1986, "Pulsatile Flow Velocity and Shear Stress Measurements in the St. Jude Valve Prosthesis," *Scandinavian Journal of Thoracic and Cardiovascular Surgery*, Vol. 20, pp. 15~28.

Yang, H. Q. and Makhijani, V. B., 1994, "A Strong Coupled Pressure-based CFD Algorithm for Fluid-Structure Interaction," *Proceeding of 32nd Aerospace Sciences Meeting and Exhibition, Reno*, NV, AIAA-94-0719.

Yoganathan, A. P., Corcoran, W. H. and Harrison, E. C., 1979, "In Vitro Velocity Measurements in the Vicinity of Aortic Prostheses," *Journal of Biomechanics*, Vol. 12, pp. 135~152.